Binary encoded computer generated holograms for temporal phase shifting

Angela Amphawan[1,2,*]

[1]*Department of Engineering Science, University of Oxford, Parks Road, Oxford, OX1 3PJ, UK*
[2]*Currently with InterNetWorks Research Group, School of Computing, Universiti Utara Malaysia, 06010 Sintok, Malaysia*
**angela@uum.edu.my*

Abstract: The trend towards real-time optical applications predicates the need for real-time interferometry. For real-time interferometric applications, rapid processing of computer generated holograms is crucial as the intractability of rapid phase changes may compromise the input to the system. This paper introduces the design of a set of binary encoded computer generated holograms (CGHs) for real-time five-frame temporal phase shifting interferometry using a binary amplitude spatial light modulator. It is suitable for portable devices with constraints in computational power. The new set of binary encoded CGHs is used for measuring the phase of the generated electric field for a real-time selective launch in multimode fiber. The processing time for the new set of CGHs was reduced by up to 65% relative to the original encoding scheme. The results obtained from the new interferometric technique are in good agreement with the results obtained by phase shifting by means of a piezo-driven flat mirror.

OCIS codes: (120.3180) Interferometry; (120.5050) Phase measurement; (120.0120) Instrumentation, measurement, and metrology; (060.0060) Fiber optics and optical communications; (280.4788) Optical sensing and sensors.

References and links

1. K. Peters, "Polymer optical fiber sensors—a review," Smart Mater. Struct. **20**(1), 1–17 (2011).
2. H. Su, M. Zervas, C. Furlong, and G. S. Fischer, "A Miniature MRI-Compatible Fiber-optic Force Sensor Utilizing Fabry-Perot Interferometer," MEMS Nanotech. **4**, 131–136 (2011).
3. V. Cortez-Retamozo, F. K. Swirski, P. Waterman, H. Yuan, J. L. Figueiredo, A. P. Newton, R. Upadhyay, C. Vinegoni, R. Kohler, J. Blois, A. Smith, M. Nahrendorf, L. Josephson, R. Weissleder, and M. J. Pittet, "Real-time assessment of inflammation and treatment response in a mouse model of allergic airway inflammation," J. Clin. Invest. **118**(12), 4058–4066 (2008).
4. T. Sibillano, A. Ancona, V. Berardi, and P. M. Lugarà, "A Real-Time Spectroscopic Sensor for Monitoring Laser Welding Processes," Sensors (Basel Switzerland) **9**(5), 3376–3385 (2009).
5. N. Kaneda, Q. Yang, X. Liu, S. Chandrasekhar, W. Shieh, and Y.-K. Chen, "Real-Time 2.5 GS/s Coherent Optical Receiver for 53.3-Gb/s Sub-Banded OFDM," J. Lightwave Technol. **28**(4), 494–501 (2010).
6. E. M. Ip and J. M. Kahn, "Fiber Impairment Compensation Using Coherent Detection and Digital Signal Processing," J. Lightwave Technol. **28**(4), 502–519 (2010).
7. B. Spinnler, "Equalizer Design and Complexity for Digital Coherent Receivers," IEEE J. Sel. Top. Quantum Electron. **16**(5), 1180–1192 (2010).
8. A. Leven, N. Kaneda, and S. Corteselli, "Real-Time Implementation of Digital Signal Processing for Coherent Optical Digital Communication Systems," IEEE J. Sel. Top. Quantum Electron. **16**(5), 1227–1234 (2010).
9. R. S. Maldonado, J. A. Izatt, N. Sarin, D. K. Wallace, S. Freedman, C. M. Cotten, and C. A. Toth, "Optimizing hand-held spectral domain optical coherence tomography imaging for neonates, infants, and children," Invest. Ophthalmol. Vis. Sci. **51**(5), 2678–2685 (2010).
10. N. Serbecic, S. C. Beutelspacher, F. C. Aboul-Enein, K. Kircher, A. Reitner, and U. Schmidt-Erfurth, "Reproducibility of high-resolution optical coherence tomography measurements of the nerve fibre layer with the new Heidelberg Spectralis optical coherence tomography," Br. J. Ophthalmol. **95**(6), 804–810 (2011).
11. S. Zotter, M. Pircher, T. Torzicky, M. Bonesi, E. Götzinger, R. A. Leitgeb, and C. K. Hitzenberger, "Visualization of microvasculature by dual-beam phase-resolved Doppler optical coherence tomography," Opt. Express **19**(2), 1217–1227 (2011).
12. W. Wieser, B. R. Biedermann, T. Klein, C. M. Eigenwillig, and R. Huber, "Multi-megahertz OCT: High quality 3D imaging at 20 million A-scans and 4.5 GVoxels per second," Opt. Express **18**(14), 14685–14704 (2010).

#152742 - $15.00 USD Received 11 Aug 2011; revised 23 Sep 2011; accepted 12 Oct 2011; published 31 Oct 2011

13. R. Tyson, *Principles of Adaptive Optics, 3rd Ed.* (CRC Press, 2011).
14. T. Kreis, *Handbook of Holographic Interferometry: Optical and Digital Methods* (Wiley-VCH, 2005).
15. D. W. Robinson, *Interferogram Analysis, Digital Fringe Pattern Measurement Techniques* (Taylor & Francis, 1993).
16. Z. Malacara and M. Servín, *Interferogram Analysis For Optical Testing, Second Edition (Optical Science and Engineering)* (CRC Press, 2005).
17. Y. Bitou, "Digital phase-shifting interferometer with an electrically addressed liquid-crystal spatial light modulator," Opt. Lett. **28**(17), 1576–1578 (2003).
18. T. Meeser, C. v. Kopylow, and C. Falldorf, "Advanced Digital Lensless Fourier Holography by means of a Spatial Light Modulator," in *3DTV-Conference: The True Vision - Capture, Transmission and Display of 3D Video (3DTV-CON), 2010* 2010), 1–4.
19. C. Falldorf, M. Agour, C. V. Kopylow, and R. B. Bergmann, "Phase retrieval by means of a spatial light modulator in the Fourier domain of an imaging system," Appl. Opt. **49**(10), 1826–1830 (2010).
20. I. W. Jung, Spatial Light Modulators and Applications Spatial Light Modulators for Applications in Coherent Communication, Adaptive Optics and Maskless Lithography *(VDM Verlag, 2009).*
21. M. A. A. Neil, T. Wilson, and R. Juskaitis, "A wavefront generator for complex pupil function synthesis and point spread function engineering," J. Microsc. **197**(3), 219–223 (2000).
22. S. Bois, *Next Generation Fibers and Standards* (Corning Optical Fiber 2009).
23. Cisco, "Cisco Visual Networking Index: Forecast and Methodology," 2009-2014 (2010).
24. J. Gowar, *Optical communication systems,* 2nd ed., Prentice-Hall international series in optoelectronics (Prentice Hall, New York, 1993), pp. xvi, 696.
25. M. B. Shemirani and J. M. Kahn, "Higher-Order Modal Dispersion in Graded-Index Multimode Fiber," J. Lightwave Technol. **27**(23), 5461–5468 (2009).
26. L. Raddatz, I. H. White, D. G. Cunningham, and M. C. Nowell, "An experimental and theoretical study of the offset launch technique for the enhancement of the bandwidth of multimode fiber links," J. Lightwave Technol. **16**(3), 324–331 (1998).
27. A. Amphawan, F. Payne, D. O'Brien, and N. Shah, "Derivation of an analytical expression for the power coupling coefficient for offset launch into multimode fiber," J. Lightwave Technol. **28**(6), 861–869 (2010).
28. K. Balemarthy, A. Polley, and S. E. Ralph, "Electronic equalization of multikilometer 10-Gb/s multimode fiber links: mode-coupling effects," J. Lightwave Technol. **24**(12), 4885–4894 (2006).
29. C. Xia, M. Ajgaonkar, and W. Rosenkranz, "On the performance of the electrical equalization technique in MMF links for 10-gigabit ethernet," J. Lightwave Technol. **23**(6), 2001–2011 (2005).
30. R. Ryf, S. Randel, A. H. Gnauck, C. Bolle, R.-J. Essiambre, P. J. Winzer, D. W. Peckham, A. McCurdy, and J. R. Lingle, "Space-division multiplexing over 10 km of three-mode fiber using coherent 6 × 6 MIMO processing," in *The Optical Fiber Communication Conference and Exposition (OFC) and the National Fiber Optic Engineers Conference (NFOEC) 2011*, 2011)
31. M. Salsi, C. Koebele, D. Sperti, P. Tran, P. Brindel, H. Mardoyan, S. Bigo, A. Boutin, F. Verluise, P. Sillard, M. Astruc, L. Provost, F. Cerou, and G. Charlet, "Transmission at 2x100Gb/s, over Two Modes of 40km-long Prototype Few-Mode Fiber, using LCOS-based Mode Multiplexer and Demultiplexer," in *The Optical Fiber Communication Conference and Exposition (OFC) and the National Fiber Optic Engineers Conference (NFOEC) 2011*, 2011)
32. A. Li, A. A. Amin, X. Chen, and W. Shieh, "Reception of Mode and Polarization Multiplexed 107-Gb/s COOFDM Signal over a Two-Mode Fiber," in *The Optical Fiber Communication Conference and Exposition (OFC) and the National Fiber Optic Engineers Conference (NFOEC) 2011*, 2011)
33. N. Hanzawa, K. Saitoh, T. Sakamoto, T. Matsui, S. Tomita, and M. Koshiba, "Demonstration of mode-division multiplexing transmission over 10 km two-mode fiber with mode coupler," in *The Optical Fiber Communication Conference and Exposition (OFC) and the National Fiber Optic Engineers Conference (NFOEC) 2011*, 2011)
34. E. Alon, V. Stojanovic, J. M. Kahn, S. Boyd, and M. Horowitz, "Equalization of modal dispersion in multimode fiber using spatial light modulators," in *GLOBECOM '04. IEEE Global Telecommunications Conference*, (IEEE, 2004), 1023- 1029.
35. P. L. Neo, J. P. Freeman, and T. D. Wilkinson, "Modal Control of a 50μm core diameter Multimode Fiber Using a Spatial Light Modulator," in *Optical Fiber Communication and the National Fiber Optic Engineers Conference, 2007. OFC/NFOEC 2007. Conference on*, (Optical Society of America, 2007), 1–3.
36. G. Stepniak, L. Maksymiuk, and J. Siuzdak, "Increasing Multimode Fiber Transmission Capacity by Mode Selective Spatial Light Phase Modulation," in *36th European Conference on Optical Communications*, 2010)
37. A. Amphawan, "Holographic mode-selective launch for bandwidth enhancement in multimode fiber," Opt. Express **19**(10), 9056–9065 (2011).
38. Thorlabs, "Tools of the Trade, Volume 20," (Thorlabs Catalogue, 2009).

1. Introduction

Interferometry is of paramount importance in diverse areas in applied physics and engineering as it provides information on the phase difference between two wavefronts and insights into the nature of electromagnetic wave propagation. Recent trends towards real-time optical applications such as optical sensors [1–4], optical transceivers [5–8] and optical tomography [9–12] predicate the need for real-time interferometry [13], even in small, lightweight,

#152742 - $15.00 USD Received 11 Aug 2011; revised 23 Sep 2011; accepted 12 Oct 2011; published 31 Oct 2011

portable devices. The observation of rapid changes in the phase is essential as it allows immediate measures to be taken at the input in order to improve the response of the system.

In temporal phase shifting interferometry, different phase shifts are induced relative to the wavefront analyzed by moving a mirror, rotating a phase plate or moving a diffraction grating [14–16]. Using interferograms recorded from the distinct phase shifts, it is possible to determine the phase of the wavefront at any measured plane [14–16]. Temporal phase shifting is typically used in stable environments. In dynamic environments with rapid fluctuations, a phase variation may take place within the time taken to record the set of interferograms, rendering the measurement invalid. The advent of spatial light modulators (SLMs) with rapid reconfiguration speed has improved interferogram recording time due to the exclusion of mechanical movement from a rotating, tilting or moving element for producing different path lengths or phase shifts with respect to the reference beam [17–19]. Instead, a more elegant approach for the generation of phase shifts is realized by simply programming the phase-shifted CGHs and then displaying them sequentially on the SLM. Amplitude [17], phase [18] and complex [19] SLMs have been used to achieve digital phase control in temporal phase shifting. Considering that a CGH is displayed almost instantaneously on the SLM [20], the time taken to program the CGH constitutes the main time constraint during the measurement of the interferograms. For adaptive real-time applications, rapid processing time of the CGH is crucial to avoid the intractability of frequent phase changes which may impede corrective measures at the input to improve the system response. For small, lightweight, portable devices such as optical sensors in handheld medical devices and optical transceivers in mobile phones and tablets, the size and weight of the device may place a constraint on the computational power of the processor. Under these circumstances, rapid processing of the CGH for temporal phase shifting in real-time applications may not be feasible. In legacy hardware with upgrade complexities, rapid processing of CGHs may also not be possible for real-time applications. Thus, it is necessary to simplify the required CGH processing in order to improve the time efficiency for interferogram recording to enable real-time processing.

The aim of this paper is to introduce the design of a set of binary encoded CGHs for five-frame temporal phase shifting interferometry based on the complex field generation technique in [21]. The CGH processing time using the new binary encoding scheme is smaller compared to the CGH processing time using the original binary encoding scheme for temporal phase shifting. This makes the new set of binary encoded CGH promising for real-time applications, particularly in small, lightweight portable devices or legacy hardware with low computational power. As a motivation for the use of the proposed design, the phase of the generated electric field for a real-time selective launch into a MMF is measured using the set of new binary encoded CGHs. The results obtained from digital temporal phase shifting using the new set of binary encoded CGHs are in good agreement with the results obtained by means temporal phase shifting using a piezo-driven flat mirror.

The paper is organized as follows. In Section 2, a mathematical derivation of the binary encoded CGH for five-frame digital temporal phase shifting is presented. An application of the binary encoded CGH for temporal phase shifting interferometry is demonstrated in a real-time selective launch into a multimode fiber in Section 3. The results from the experimental demonstration of the use of the new binary encoded CGHs for temporal phase shifting are then presented in Section 4. Finally, in Section 5, the results from the new digital phase shifting design are compared with results from standard mechanical phase shifting using a piezo-driven flat mirror.

2. Mathematical derivation of binary encoded CGH for temporal phase shifting

For conventional temporal phase shifting, distinct phase shifts are induced in the reference beam with respect to the analyzed wavefront. To accomplish the same effect in digital temporal phase shifting, the phase of the reference beam is preserved while distinct phase shifts are added to the analyzed wavefront. For each distinct phase shift between the wavefront analyzed and the reference beam, an interferogram of the phase-shifted wavefront

#152742 - $15.00 USD Received 11 Aug 2011; revised 23 Sep 2011; accepted 12 Oct 2011; published 31 Oct 2011

and the constant reference beam is recorded on a particular plane. For five-frame temporal phase shifting, the intensities of the interferograms are given by [15-16]:

$$I_1 = I_o\left[1+\gamma\cos(\phi-2p)\right] \tag{1}$$

$$I_2 = I_o\left[1+\gamma\cos(\phi-p)\right] \tag{2}$$

$$I_3 = I_o\left[1+\gamma\cos\phi\right] \tag{3}$$

$$I_4 = I_o\left[1+\gamma\cos(\phi+p)\right] \tag{4}$$

$$I_5 = I_o\left[1+\gamma\cos(\phi+2p)\right] \tag{5}$$

where ϕ is the phase of the test beam, γ is the fringe visibility, in radians and $p = \pi/2$ radians is the induced phase shift.

The phase from the five interferograms is given by [15-16]:

$$\phi = \tan^{-1}\left\{2\left(I_2 - I_4\right)/\left[2I_3 - I_5 - I_1\right]\right\} \tag{6}$$

The relative phase shifts between the wavefront analyzed and the constant reference beam for the five interferograms in Eqs. (1) to (5) are $\sigma = -\pi, -\pi/2, 0, \pi/2$ and π respectively.

In [21], a complex field was generated using a binary amplitude SLM. For temporal phase shifting of the generated complex wavefront in [21], four distinct phase shifts $\sigma = -\pi, -\pi/2, \pi/2$ and π may be added separately to the generated complex wavefront, followed by the binary encoding of each of the phase-shifted tilted wavefront. However, for small, lightweight, portable devices such as optical sensors in medical devices and optical transceivers in mobile phones and tablets, the size and weight of the device may place a constraint on the computational power and storage used in the processor. In legacy hardware with upgrade complexities, rapid processing of CGHs may also not be possible for real-time applications. Under such circumstances, it is necessary to simplify the required CGH processing in [21] in order to improve the time efficiency for interferogram recording. This is achieved by separate encoding schemes for different phase-shifted fields. Using the original encoding scheme, the calculation of the phase-shifted modal fields for the different phase shifts may be computationally expensive and increases the execution time for temporal phase shifting. Considering that a CGH is displayed almost instantaneously on the SLM [20], the time taken to program the CGH constitutes the main time constraint during the measurement of the interferograms. For real-time applications, the processing time for the CGH is crucial to avoid intractability of rapid phase changes and inaccurate feedback to the input. Thus, the proposed encoding scheme is a more direct approach for temporal phase shifting. A comparison of the use of the original encoding scheme and the proposed technique is shown in Fig. 1.

The simplified phase mappings of the required phase shifts onto the binary CGH based on the complex wavefront generation technique in [21] will be derived as follows. Let the required phase shift relative to the fixed reference beam,

$$\sigma = -\pi. \tag{7}$$

After the addition of linear tilts in the x and y directions to the phase of the desired field, ξ and the required phase shift, σ, the new tilted wavefront is given by

#152742 - $15.00 USD Received 11 Aug 2011; revised 23 Sep 2011; accepted 12 Oct 2011; published 31 Oct 2011

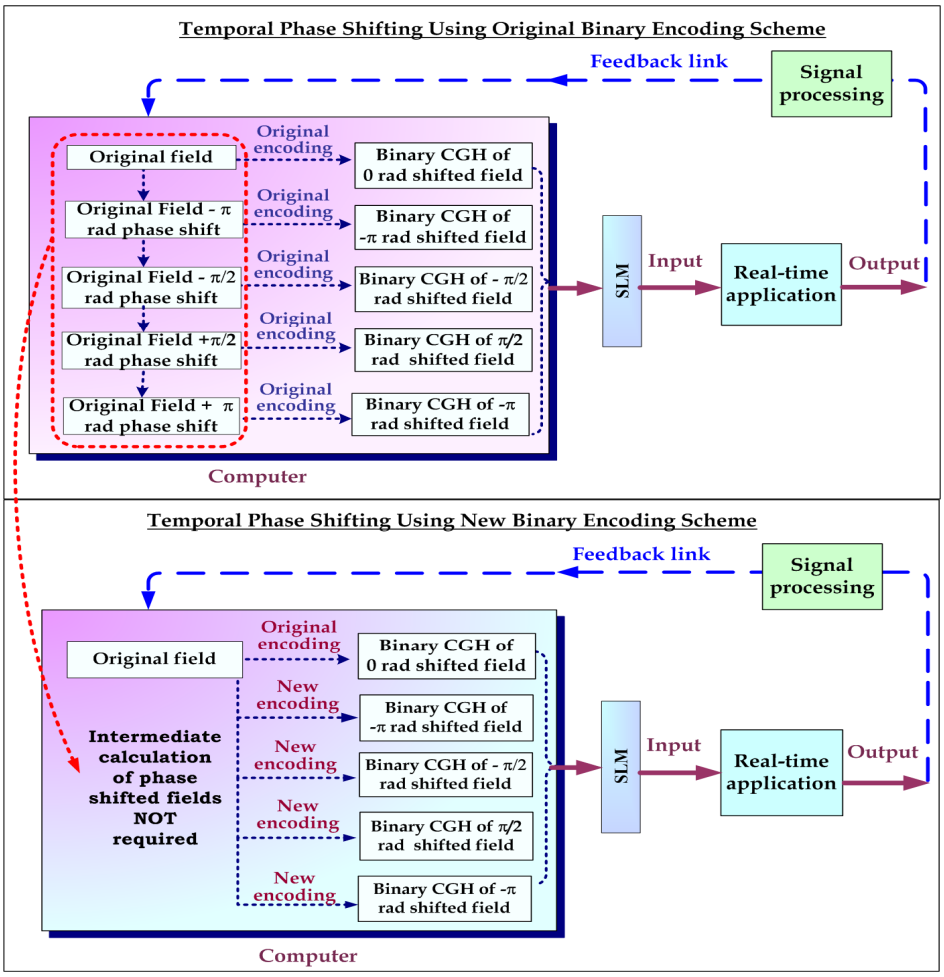

Fig. 1. Comparison of new set of binary encoding scheme and original binary encoding scheme for five-frame temporal phase shifting in real-time applications

$$f(x) = a(x)\exp[j(\xi(x,y) + \tau_x x + \tau_y y + \sigma)] \tag{8}$$

where $a(x, y)$ is the amplitude of the field and ξ is the phase of the field. Let

$$u = \mathrm{Re}\{f(x,y)\},\ v = \mathrm{Im}\{f(x,y)\}, \tag{9}$$

then

$$u = a(x,\ y)\cos\left[\xi(x,y) + \tau_x x + \tau_y y + \sigma\right] \tag{10}$$

$$v = a(x,\ y)\sin\left[\xi(x,y) + \tau_x x + \tau_y y + \sigma\right] \tag{11}$$

$$\left|a(x,\ y)\right| = \sqrt{u^2 + v^2} \tag{12}$$

The binarized output, $g(x, y)$ is *1* when the total phase is less than α,

$$\xi + \tau_x x + \tau_y y + \sigma \le \alpha \tag{13}$$

where α is a constant. Taking the sine of both sides of Eq. (13),

#152742 - $15.00 USD Received 11 Aug 2011; revised 23 Sep 2011; accepted 12 Oct 2011; published 31 Oct 2011

$$\sin\left(\xi+\tau_x x+\tau_y y+\sigma\right)\le \sin\alpha \tag{14}$$

$$\text{given}\quad -\pi/2\ \le\ \xi+\tau_x x+\tau_y y+\sigma\ \le\ \pi/2 \tag{15}$$

$$0\le\alpha\le\ \pi/2 \tag{16}$$

for the sine function to be monotonically increasing.

From the Fourier series expansion of the binarized output, *G(x, y)*, given in the first harmonic (n = 1) has an amplitude,

$$a(x)=\sin\ \alpha \tag{17}$$

L1 Fourier transforms the first harmonic into the first diffraction order in the focal plane of the *L1*. The first diffraction order is Fourier transformed again by *L2*, and the image in the back focal plane of *L2* is also has amplitude of $a(x)=\sin\ \alpha$.

Combining Eqs. (11), (12) (14) and (17),

$$\left(v\pm\frac{1}{2}\right)^2+u^2\ge\ \frac{1}{4},\ u\le 0 \tag{18}$$

In the same manner, the phase mappings for relative phase shifts, $\sigma=-\pi/2,\ \pi/2$ and π with respect to the fixed reference beam were derived. The following inequalities are the results of the derived phase mappings for $\sigma=-\pi/2,\ \pi/2$ and π phase shifts respectively:

$$\left(u\pm\frac{1}{2}\right)^2+v^2\ge\frac{1}{4},\ v\ge 0 \tag{19}$$

$$\left(u\pm\frac{1}{2}\right)^2+v^2\ge\frac{1}{4},\ v\le 0 \tag{20}$$

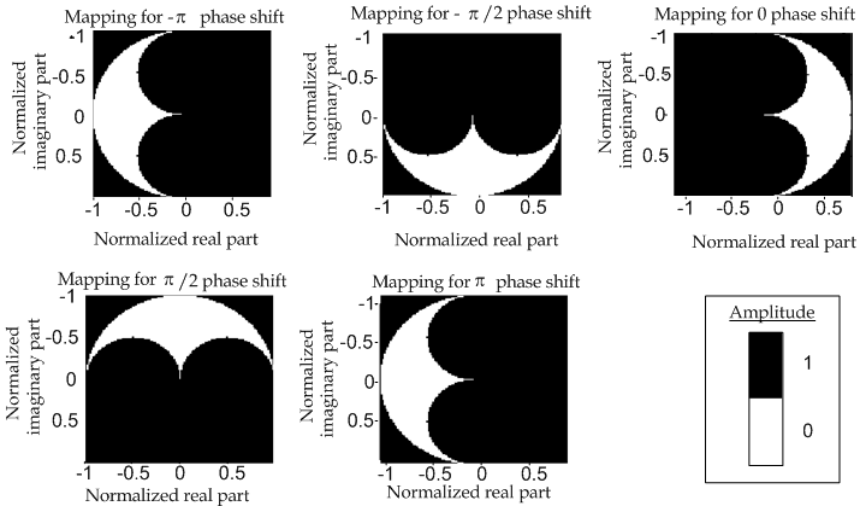

Fig. 2. Encoding of normalized complex plane onto a binary CGH for -π, -π/2, 0, π/2 and π phase shifts relative to a fixed reference beam. Amplitude of *0* and *1* indicate intensity transmission and no intensity transmission respectively through a pixel in the SLM active area

#152742 - $15.00 USD Received 11 Aug 2011; revised 23 Sep 2011; accepted 12 Oct 2011; published 31 Oct 2011

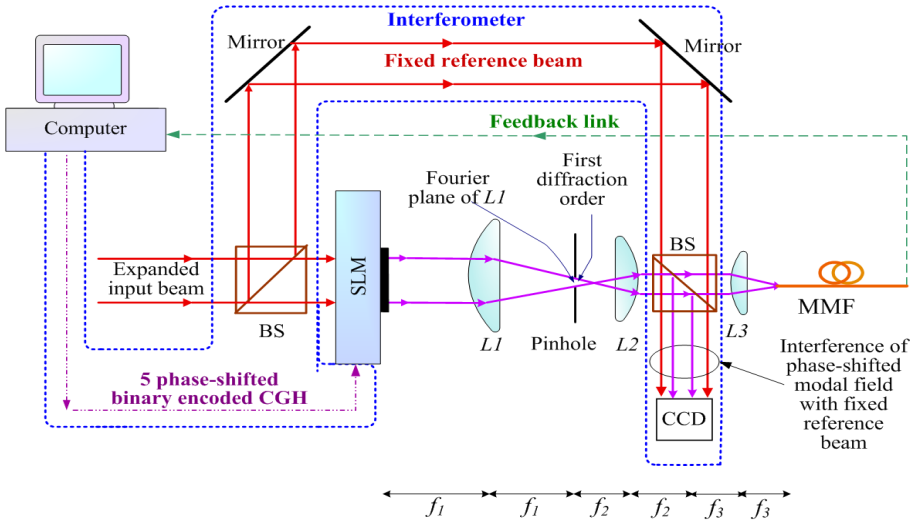

Fig. 3. Digital temporal phase shifting using binary encoded CGHs for a real-time selective launch into a MMF

$$\left(v \pm \frac{1}{2}\right)^2 + u^2 \geq \frac{1}{4},\ u \leq 0 \tag{21}$$

The complex plane mappings of the tilted modal electric field onto a binarized hologram are shown in Fig. 2 for -π, -π/2, 0, π/2 and π phase shifts relative to a fixed reference beam.

3. Demonstration of application of binary encoded CGH for temporal phase shifting

As a motivation for the use of the proposed binary CGH, the phase of the generated electric field for a real-time selective launch in multimode fiber (MMF) is measured by temporal phase shifting using the new set of binary encoded CGHs. In Local Area Networks, MMF is the conventional choice for supporting high bandwidth links [22]. For optimum bandwidth enhancement in order to meet rapidly increasing customer demands [23], it is necessary to curtail modal dispersion in MMF [24-25]. Confinement of the channel to the least possible number of modes is desirable and may be achieved by selective launches which excite only a subset of propagating modes [26–33]. Recently, selective launches into MMF have been achieved by employing spatial light modulators (SLMs) [31, 34–37]. In selective launches, prior to coupling the generated modal field into the MMF, it is valuable to verify the phase of the generated electric field to maximize power coupling efficiency. This is to ensure optimum bandwidth enhancement in the channel. In selective launches with the SLM as the modal field generator, a digital temporal phase shifting interferometer may be easily constructed using the existing SLM.

The experimental setup for the real-time selective launch into a MMF based on the experiment in [37] is shown in Fig. 3 The additional parts required for the temporal phase shifting interferometer are outlined in blue. A 128x128 pixel transmissive binary amplitude spatial light modulator (SLM), two achromatic doublets [focal lengths f_1 = 300mm (*L1*) and f_2 = 100mm (*L2*)] and a fiber collimator with an aspheric lens of f_3 = 11mm (*L3*) were used. A visible 632.8nm Helium Neon laser was used to easily view modal field at various points along the system and to easily capture the interferograms. The MMF used was a 1km-long graded-index Thorlabs GIF625 [38], with a core diameter of 62.5μm

#152742 - $15.00 USD Received 11 Aug 2011; revised 23 Sep 2011; accepted 12 Oct 2011; published 31 Oct 2011

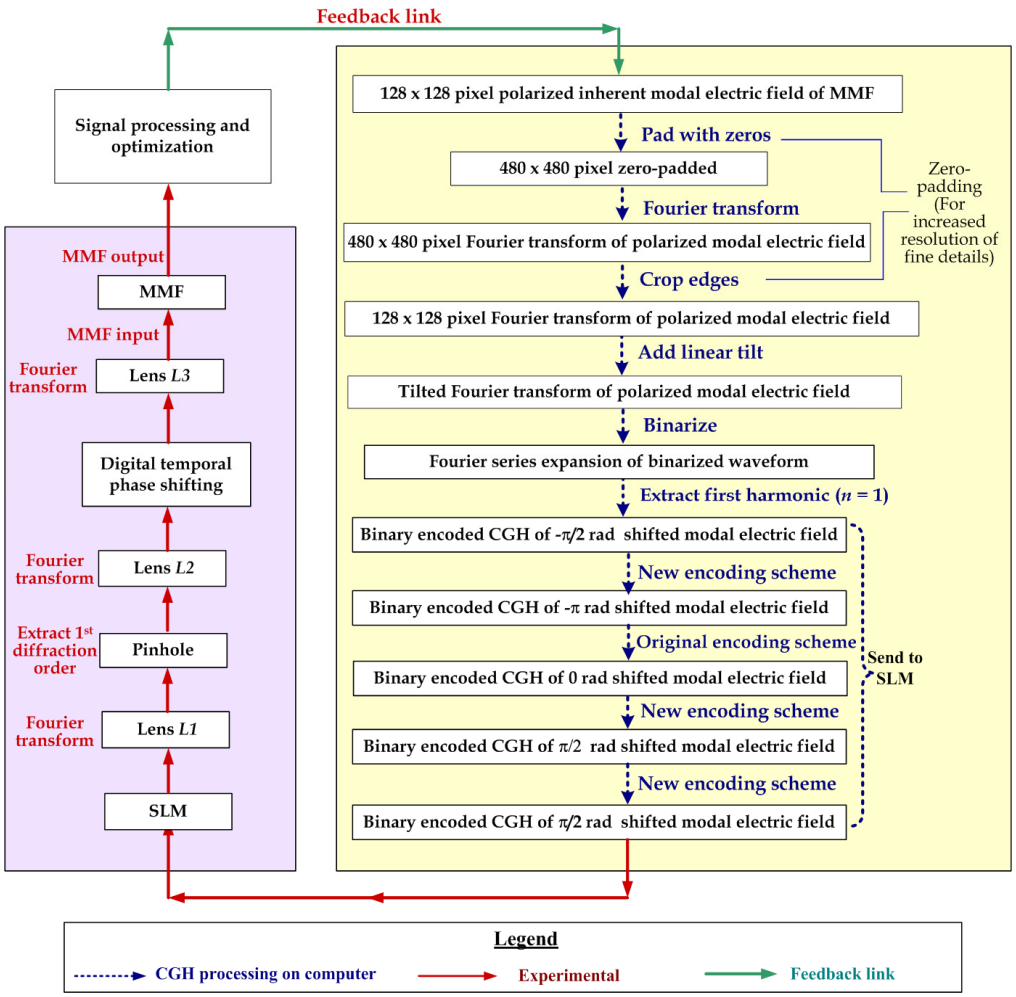

Fig. 4. Summary of technique used for selective launch in MMF, adapted from [37]

The expanded laser beam from the beam expander was split into two optical paths, as shown in Fig. 3. The first optical path was used for generating the modal electric field to be coupled into the MMF while the second optical path was used as a fixed reference beam for the interferometry.

The technique used for generating the electric field is illustrated in Fig. 4 and is summarized here. First, the desired electric field $c(x_1, y_1)$ was Fourier transformed, with zero-padding to increase the resolution of fine details. Next, a linear tilt of $\tau_x = 88\pi$ in the horizontal direction and $\tau_y = 120\pi$ in the vertical direction was added to the resultant field [21]. These tilt values were chosen as they provided sufficient spatial separation of the diffraction orders in the Fourier plane so that the first diffraction order may be easily extracted later. This yielded the complex field:

$$f(x_1, y_1) = d(x_1, y_1) \exp\left[j(\tau_x x_1 + \tau_y y_1)\right] \tag{22}$$

where x_1 and y_1 are spatial coordinates of the Fourier transformed field in the Fourier plane; and $d(x_1, y_1)$ is the Fourier transform of the polarized modal electric field.

The complex field $d(x_1, y_1)$ may be binarized by first mapping the space of possible phase values ϕ on the space g of binarized ones $g(\phi)$: $x \rightarrow g(\phi)$ using:

#152742 - $15.00 USD Received 11 Aug 2011; revised 23 Sep 2011; accepted 12 Oct 2011; published 31 Oct 2011

$$\phi = \xi(x_1, y_1) + \tau_x x_1 + \tau_y y_1 \tag{23}$$

where $\xi(x_1, y_1)$ is the phase of the Fourier transform of the polarized modal electric field. Then, the real part of Eq. (22) is taken and approximated by a Fourier series given by the following expression:

$$g(\phi) = \frac{a_o}{2} + \sum_{n=1}^{\infty} [\, a_n \cos(n\phi) + b_n \sin(n\phi)\,] \tag{24}$$

where a_o is the constant term and a_n is the Fourier cosine coefficient, b_n is the Fourier sine coefficient. Only the real part of the complex field d (x_1, y_1) is required, thus $b_n = 0$. Substituting Eq. (23) into Eq. (24) yields

$$\hat{g}(x_1, y_1) = g(\phi)\big|_{(x_1, y_1)} = \frac{a_o}{2} + \sum_{n=1}^{\infty} a_n \cos(n\phi) \tag{25}$$

This gives the binarized CGH function:

$$\hat{g}(x_1, y_1) = \frac{a_o}{2} + \frac{4}{\pi} \sum_{n=1}^{\infty} a_n \cos\left\{ n[\xi(x_1, y_1) + \tau_x x_1 + \tau_y y_1] \right\} \tag{26}$$

The binarized CGH function was displayed on the SLM. This was then Fourier transformed by *L1*. From Eq. (26), the Fourier transformed field in the back focal plane or Fourier plane of *L1* is given as:

$$\hat{G}(x_2, y_2) = M_o(x_2, y_2) + \sum_{n=1}^{\infty} [M_n(x_2 + n\tau_x,\ y_2 + n\tau_y) + M_n^*(n\tau_x - x_2, n\tau_y - y_2)] \tag{27}$$

where x_2 and y_2 are spatial coordinates in the Fourier plane of *L1*, * is the complex conjugate and $M_n(x_1, y_1)$ is the *n*-th diffraction order.

The first diffraction order, M_1 was then spatially filtered using a pinhole located in the back focal plane of *L1*. The combination of *L2* and *L3* then scales M_1. Following this, the generated modal field was then interfered with the reference beam in the back focal plane of *L2*. This was the closest location possible for the interference as *L3* was connected directly to the input endface of the MMF using a fiber collimator [38]. The five binary encoded CGHs described in the previous section were displayed on the SLM sequentially to generate five interferograms of the phase-shifted electric field with respect to the reference beam.

In this experiment, five frames were the minimum number of frames for producing satisfactory phase shift distribution. When three and four frames were used for phase shifting, many errors were found in peripheral regions where intensity values were low.

4. Experimental results

Five measured interferograms of the phase-shifted electric fields with respect to the reference field are shown in Fig. 5 (a-e). The phase was then retrieved from the five interferograms using Eq. (6). The retrieved phase distribution is shown in Fig. 5(f). The experiment was repeated three times for each mode excited and the mean squared error (*MSE*) between the retrieved phase distributions were calculated using:

$$MSE = \frac{1}{pq} \sum_{t=1}^{p} \sum_{u=1}^{q} \left[\theta_1(t,u) - \theta_2(t,u) \right]^2 \tag{28}$$

where θ_1 is the phase distribution from the first measurement, θ_2 is the phase distribution from the second measurement, *t* is the index number for pixels on the horizontal axis, *u* is the index number for pixels on the vertical axis, $p = 128$ is the total number of pixels on the horizontal axis, and $q = 128$ is the total number of pixels on the vertical axis. Using Eq. (28), the MSEs

#152742 - $15.00 USD Received 11 Aug 2011; revised 23 Sep 2011; accepted 12 Oct 2011; published 31 Oct 2011

of the second and third measured phase distributions relative to the first measured phase distribution were 0.014 and 0.009 respectively.

The relative power coupled into a fiber mode of a weakly guiding infinite parabolic MMF is given by the power coupling coefficient,

$$\eta_{lm} = \left| \iint_{A_{core}} \mathbf{E}_{inc}(x,y)\ \mathbf{e}_t{}^*(x,y)dxdy \right|^2 \Bigg/ \iint_{A_{core}} \left|\mathbf{E}_{inc}(x,y)\right|^2 dxdy \iint_{A_{core}} \left|\mathbf{e}_t(x,y)\right|^2 dxdy \quad (29)$$

where e_t is the transverse field of a fiber mode, E_{inc} is the incident electric field of the offset beam and A_{core} is the cross sectional area of the fiber core. In the experimental setup in the power coupling efficiency is sensitive to the pitch, yaw, roll and distance of the SLM and lens with respect to the MMF. By measuring the phase at the end of the MMF prior to the launch, it is possible to adjust the pitch, yaw, roll and distance of the SLM and lens with respect to the MMF individually to find optimum power coupling into the desired mode.

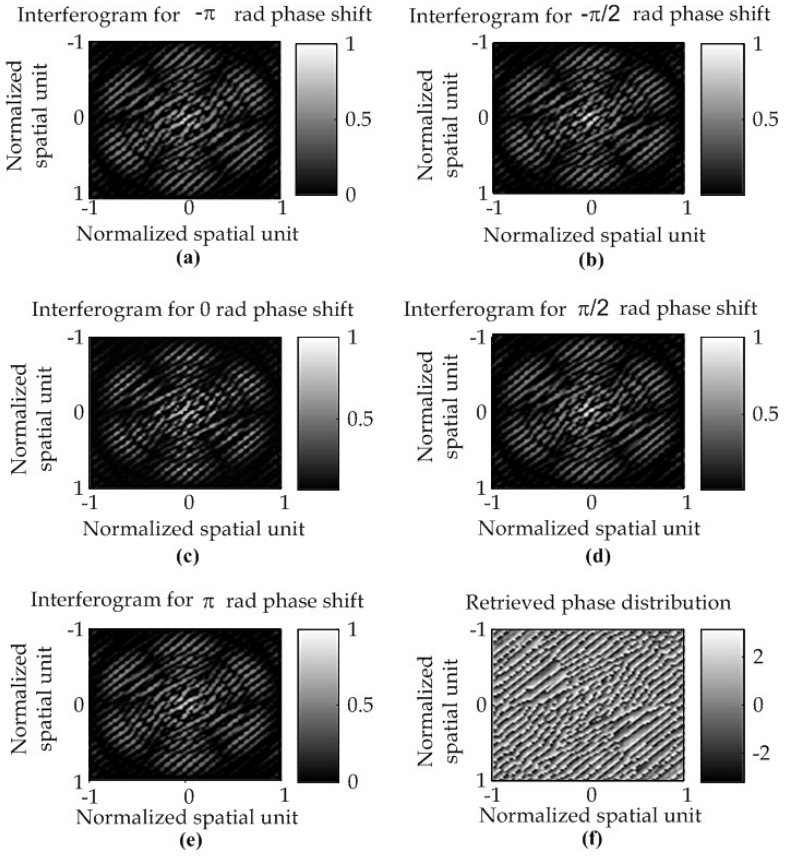

Fig. 5. (a-e) Interferograms from digital phase shifting technique using new binary encoded CGHs (f) Retrieved phase distribution using new digital phase shifting technique

#152742 - $15.00 USD Received 11 Aug 2011; revised 23 Sep 2011; accepted 12 Oct 2011; published 31 Oct 2011

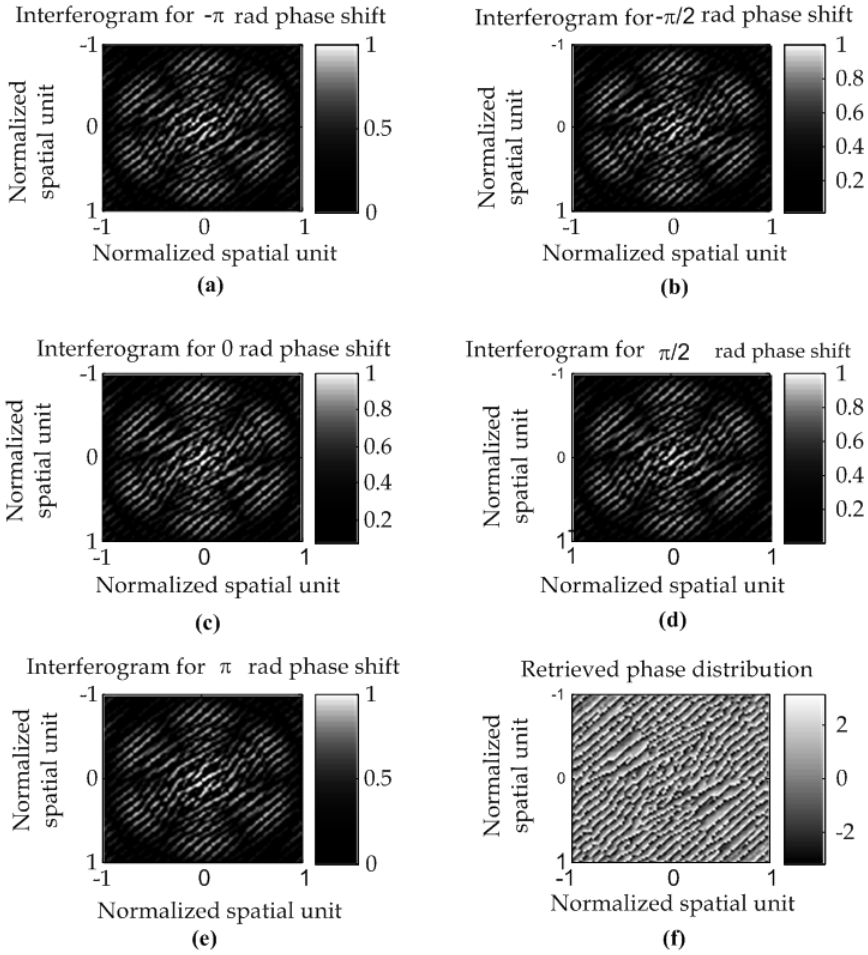

Fig. 6. (a-e) Interferograms using a flat mirror shifted by a piezo drive. (f) Retrieved phase distribution temporal phase shifting using a flat mirror shifted by a piezo drive.

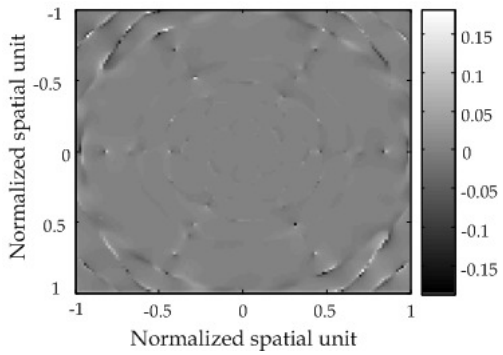

Fig. 7. Phase difference (radians) between digital phase shifting using new binary encoded CGHs and mechanical digital phase shifting using piezo-driven mirror

5. Comparison to mechanical temporal phase shifting

The phase distribution obtained from the new set of binary CGHs using a binary amplitude SLM is compared to the phase distribution obtained from mechanical temporal phase shifting

#152742 - $15.00 USD Received 11 Aug 2011; revised 23 Sep 2011; accepted 12 Oct 2011; published 31 Oct 2011

using a piezo-driven flat mirror. The measured phase distribution from mechanical temporal phase shifting using a flat mirror is shown in Fig. 6. It is found that the measured phase distribution from the new binary CGH is in good agreement with the measured phase distribution from mechanical temporal phase shifting, as shown in Fig. 7. The maximum phase difference is 0.18 rad. The discrepancy may be due to slight vibrations, air movement as well as thermal and electrical fluctuations in the sensor system. In peripheral regions, the discrepancy is higher as the slight environmental fluctuations have a more prominent effect on the low-intensity values in the interferograms, contributing to a higher error in the phase calculation, as evident in Fig. 7. The CGH processing time was reduced by 50% to 65% relative to the original encoding scheme when the new encoding scheme was used.

6. Conclusion

The design of a set of binary encoded computer generated holograms (CGHs) for five-frame temporal phase shifting interferometry using a binary transmissive amplitude SLM is presented. The new set of binary encoded CGHs is suitable for real-time applications in portable devices or legacy hardware with constraints in computational power. To demonstrate a practical application for this, the phase of the generated electric field for a real-time selective launch in MMF is measured by temporal phase shifting using the new binary encoded CGHs. The CGH processing time was reduced by 50% to 65% relative to the original encoding scheme when the new encoding scheme was used. The results obtained from the new binary encoded CGHs are in good agreement with the results obtained by phase shifting by means of a piezo-driven flat mirror.

Acknowledgement

The author would like to thank Dr. Dominic O'Brien, Dr. Frank Payne and Dr. Martin Booth at the University of Oxford for their important advice and feedback.

#152742 - $15.00 USD Received 11 Aug 2011; revised 23 Sep 2011; accepted 12 Oct 2011; published 31 Oct 2011